New SND results on the light hadron spectroscopy including 2π and multi hadron channels

Kupich Andrey

Budker Institute of Nuclear Physics,
Novosibirsk State University

on behalf of the SND collaboration

Muon g-2 theory initiative workshop. June 28 – July 2, 2021
Japan

VEPP-2000 e^+e^- collider

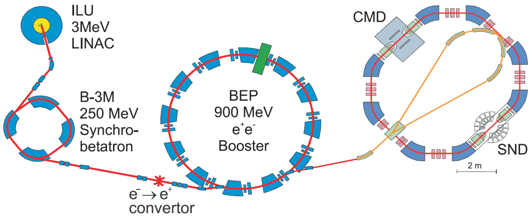

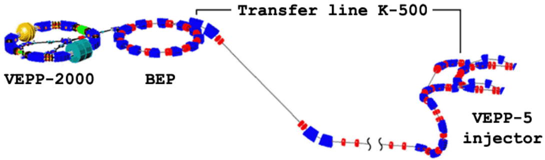

VEPP-2000 parameters

- c.m. energy E=0.3-2.0 GeV
- Luminosity at E=1.8 GeV
  $10^{32} cm^{-2} sec^{-1}$ (project)
  $4x10^{31} cm^{-2} sec^{-1}$ (achieved)
- Beam energy spread - 0.6 MeV at E=1.8 GeV

- 10 times more intense positron source
- Experiments at upgraded VEPP-2000 was restarted by the end of 2016

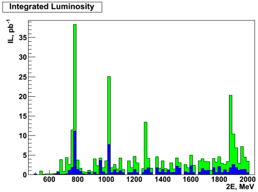

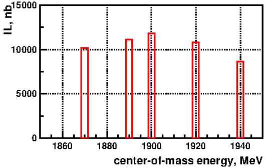

Timeline

2010-2013 – experiments, 70 pb^{-1}
2013-2016 – upgrade, new injector
2016-2019 – experiments, 210 pb^{-1}
2020 – 50 pb^{-1} collected in two months, before lockdown

Most recent results published

- $e^+e^- \to K^+K^-\pi^0$
- $e^+e^- \to \pi^+\pi^-\pi^0$
- $e^+e^- \to \eta\pi^0\gamma$
- $\mathbf{e^+e^- \to \pi^+\pi^-}$
- $e^+e^- \to f_1(1285)$

$e^+e^- \to \pi^+\pi^-$ analysis is based on the **4.6 pb^{-1}** statistics, collected in 2012 – 2013, that corresponds to the **2.3** $\times$ **10^6** collinear events, with **10^6** $e^+e^- \to \pi^+\pi^-, \mu^+\mu^-$ and **1.3** $\times$ **10^6** $e^+e^- \to e^+e^-$

SND detector

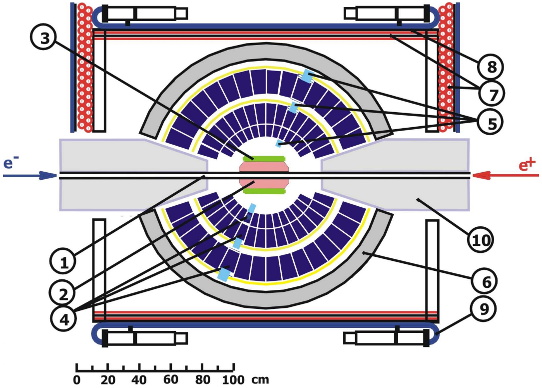

1-beam pipe, **2**-tracking system, **3**- aerogel Cherenkov counter , **4** - NaI(Tl) crystals, **5** - phototriodes, **6** - iron muon absorber, **7-9** - muon detector, **10** - focusing solenoids.

Main physics task of SND is study of all possible processes of e^+e^- annihilation into hadrons below 2 GeV.

- The total hadronic cross section, which is calculated as a sum of exclusive cross sections.
- Study of hadronization (dynamics of exclusive processes).
- Study of the light vector mesons.
- Production of the C-even resonances

$e^+e^- \to f_1(1285)$

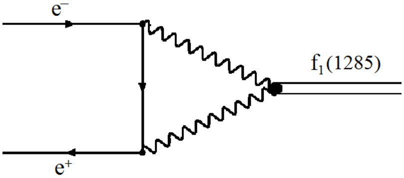

$B(f_1(1285) \to e^+e^-)$ is calculated using cross section of the $e^+e^- \to f_1(1285)$ process. Theory predicts $B(f_1(1285) \to e^+e^-) = 3.5 \pm 1.8 \times 10^{-9}$

$e^+e^- \to f_1(1285)$

- 2010–2012 and 2017 data are used.
- IL=15 pb^-1 in 1.2 GeV $\leq \sqrt{s} \leq$ 1.4 GeV.
- About 3.4 pb^{-1} of data were collected in the resonance maximum.
- The $f_1(1285) \to \pi^0\pi^0\eta \to 6\gamma$ decay mode is used, with 1% efficiency.
- The main background sources are $e^+e^- \to \omega\pi^0 \to \pi^0\pi^0\gamma$, $e^+e^- \to \eta\gamma$ and $e^+e^- \to \pi^0\pi^0\omega$.
- After applying the selection criteria, two events have been observed at the peak (with 0.25 expected background events).
- 0 events selected outside the $f_1(1285)$ peak.
- These two events correspond to $B(f_1(1285) \to e^+e^-) = 5.1^{+3.7}_{-2.7} \times 10^{-9}$ and have 2.5 σ.

Phys. Lett. B800 (2020) 135074

$e^+e^- \to \pi^+\pi^-\pi^0$ at $\sqrt{s} > 1.05$ GeV

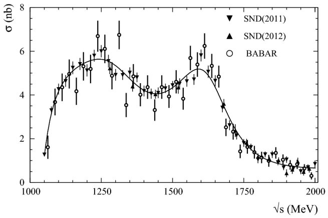

The total $e^+e^- \to \pi^+\pi^-\pi^0$ cross section was measured by SND in $\sqrt{s}$ =1.05–2 GeV energy region (**IL = 34pb^{-1}**) with **4.4%** systematic uncertainty. Main contributions coming from the $\omega(1420)$ and $\omega(1650)$.

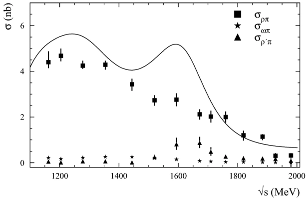

Eur.Phys.J. C80 (2020) no.10, 993

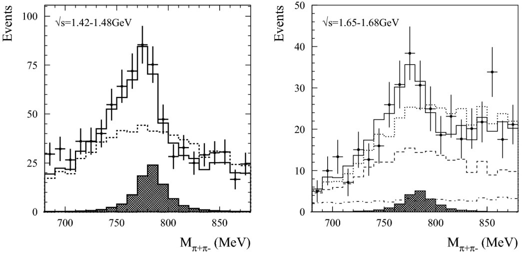

Exclusive channels at $\sqrt{s} > 1.15$ GeV (IL = 28pb^{-1})

- Subprocesses $\mathbf{e^+e^- \to \rho(770)\pi, \rho(1450)\pi, \omega\pi}$ ($\rho\pi : \rho^0\pi^0, \rho^-\pi^+, \rho^+\pi^-$) were studied, using $M_{\pi^+\pi^-}$.
- Contribution of each channel was measured.
- $\boldsymbol{\omega(1420) \to 3\pi}$ is dominated by $\boldsymbol{\omega(1420) \to \rho(770)\pi}$.
- $\boldsymbol{\omega(1650) \to \rho(1450)\pi}$ channel plays a major role in $\boldsymbol{\omega(1650) \to 3\pi}$

$e^+e^- \to K^+K^-\pi^0$

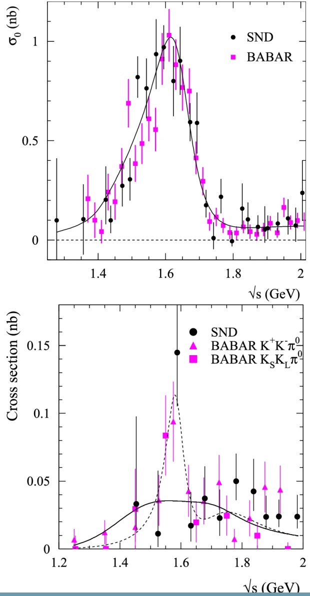

$e^+e^- \to K^+K^-\pi^0$ was studied by SND in $\sqrt{s}$ =1.27–2 GeV energy region (**IL = 26pb^{-1}**)

Cross sections of the $\mathbf{e^+e^- \to K^{*\pm}K^{\mp} \to K^+K^-\pi^0}$ and $\mathbf{e^+e^- \to \phi\pi^0 \to K^+K^-\pi^0}$ are measured separately.

- $\mathbf{e^+e^- \to K^{*\pm}K^{\mp} \to K^+K^-\pi^0}$ is dominated by ϕ**(1680)** decay.
- Fit of the $\mathbf{e^+e^- \to \phi\pi^0 \to K^+K^-\pi^0}$ cross section (with BABAR data) shows the presence of additional resonance (3σ) with **m = 1585 ± 15MeV** and **Γ = 75 ± 30MeV**.

Eur.Phys.J. C80 (2020) no.12, 1139

$e^+e^- \to \eta\pi^0\gamma$

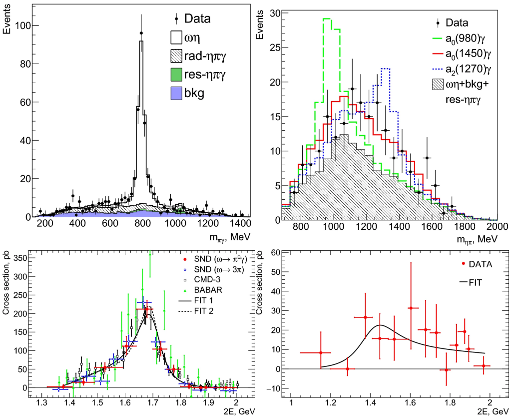

$e^+e^- \to \eta\pi^0\gamma$ was studied by SND in $\sqrt{s}$ =1.05–2 GeV energy region ($\mathbf{IL = 95pb^{-1}}$)

$\mathbf{e^+e^- \to \eta\pi^0\gamma}$ are dominated by $\mathbf{e^+e^- \to \eta\omega}$ with additional contributions from $\eta\phi$, $\eta\rho$, $\phi\pi^0$, $\omega\pi^0$ and possible $a_0\gamma$ radiative decays.

- $e^+e^- \to \omega\eta \to \eta\pi^0\gamma$ can be described with $\omega(1420)$ and $V''(1680)$.
- It is found, with a significance of 5.6 σ, that the process $\mathbf{e^+e^- \to \eta\pi^0\gamma}$ is not completely described by hadronic vector-pseudoscalar intermediate states.
- Cross section of the $e^+e^- \to a_0(1450)\gamma$ was measured.

Eur.Phys.J. C80 (2020) no.11, 1008.

Measurement of the $\mathbf{e^+e^-} \to \boldsymbol{\pi^+\pi^-}$ cross section in the energy region $0.525 < \sqrt{s} < 0.883$ GeV

Events selection

1. $N_{ch} \geq 2$. The events can contain neutral particles due to nuclear interactions of charged pions with detector material or due to electromagnetic showers splitting
2. $|\Delta\theta| = |180^\circ - (\theta_1 + \theta_2)| < 12^\circ$ and $|\Delta\phi| = |180^\circ - |\phi_1 - \phi_2|| < 4^\circ$, where ϕ is the particle azimuthal angle
3. $E_{1,2} > 40$ MeV, where E_i is the ith particle $(i = 1, 2)$ energy deposition
4. $50^\circ < \theta_0 = (\theta_1 - \theta_2 + 180^\circ) \times 0.5 < 130^\circ$
5. $|d0_1| < 1$ cm , $|d0_2| < 1$ cm, where $|d0_i|$ is a distance between the ith particle track and the beam axis
6. $|z0_1| < 8$ cm , $|z0_2| < 8$ cm, where $|z0_i|$ is a distance from the center of the detector to the primary vertex of the ith particle track along the beam axis
7. The muon system $veto = 0$

The output signal of the trained BDT network R is a value in the interval from -1.0 to 1.0

The $e^+e^- \to e^+e^-$ events are located in the region $R < 0$, while $e^+e^- \to \pi^+\pi^-, \mu^+\mu^-$ events in $R > 0$.

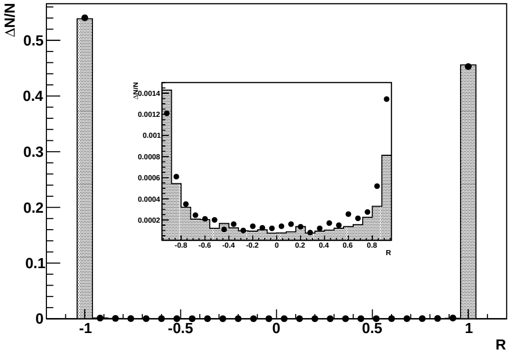

Non-collinear and cosmic backgrounds

$$N_{cosm} = N_{exp}[veto = 1] \times \frac{N_{cosm}[veto = 0]}{N_{cosm}[veto = 1]}$$

$N_{exp}[veto = 1]$ – number of data events selected with 2π cuts but with veto=1;
$N_{cosm}[veto = 0(1)]$ – number of special cosmic events

Two types of cosmic events are used:

- Non-central ($|d0_1| > 0.5$ cm , $|d0_2| > 0.5$ cm, $|z0_1| > 5$ cm and $|z0_2| > 5$ cm) events from the same data sample.
- Events from special cosmic runs without beams

Both give the **same 2.5%** ratio between $N_{cosm}[veto = 0]$ and $N_{cosm}[veto = 1]$ in **every energy point**

Non-collinear and cosmic backgrounds

Background from the $e^+e^- \to \pi^+\pi^-\pi^0$ is subtracted directly in the $\omega(782)$ region, with a number of background events estimated according to the formula:

$$N_{3\pi} = N^{exp}[3\pi] \times \frac{N_{3\pi}^{mc}[2\pi]}{N_{3\pi}^{mc}[3\pi]}$$

$N^{exp}[3\pi]$ – number of $e^+e^- \to \pi^+\pi^-\pi^0$ events in the same data sample selected with a special 3π cuts:

$$N_{cha} \geq 2,\ N_n \geq 2,\ |\Delta\theta| > 10^\circ,\ |\Delta\phi| > 10^\circ,\ 40^\circ < \theta_i < 140^\circ,\ \chi^2_{\pi^+\pi^-\pi^0} < 30$$

Contribution of this background to the total $e^+e^- \to \pi^+\pi^-$ cross section **is less than 0.15%**, due to the strong suppression by $|\Delta\theta|$ and $|\Delta\phi|$ cuts.

ID efficiency

$$\varepsilon_e = \frac{N^{ee}(R \in [-1;0])}{N^{ee}(R \in [-1;1])}, \quad \varepsilon_\pi = \frac{N^{\pi\pi}(R \in [0;1])}{N^{\pi\pi}(R \in [-1;1])}$$

$N^{ee,\pi\pi}(R \in [a;b])$ are the numbers of $e^+e^- \to e^+e^-$ or $\pi^+\pi^-$ events with R in the interval $[a;b]$

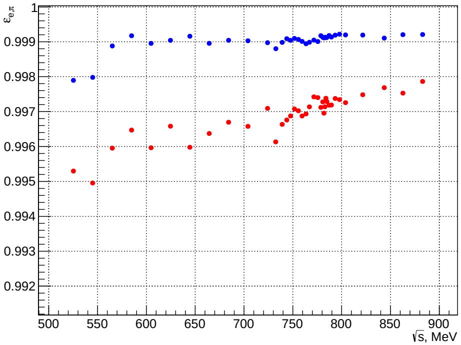

Identification efficiencies for $e^+e^- \to e^+e^-$ and $e^+e^- \to \pi^+\pi^-$ simulated events

ID efficiency correction

$$\delta_x = \frac{\epsilon_x^{exp}}{\epsilon_x^{mc}}$$

$x = e(\pi)$, ϵ_x^{exp} and ϵ_x^{mc} are identification efficienties for experimental and simulated pseudoevents respectively. The δ_e does not depend on energy, and its average value is 1.0006 ± 0.0001

$$\delta_\pi(\sqrt{s}) = a\left(\sqrt{(\sqrt{s}-b)^2+10}-(\sqrt{s}-b)\right)+c$$

$\delta_\pi = 0.9990 \pm 0.0002$ at the energy region $\sqrt{s} > 0.65$ GeV and below δ_π changes upto 0.9950 ± 0.0006 at $\sqrt{s} = 0.52$ GeV

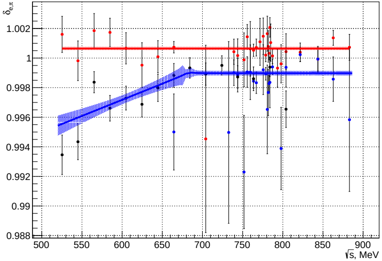

Correction coefficients for ID efficiencies of the $e^+e^- \to e^+e^-$ and $e^+e^- \to \pi^+\pi^-$ events. δ_π obtained using pseudo $\pi\pi$ events constructed from $e^+e^- \to \pi^+\pi^-$ and $e^+e^- \to \omega, \phi \to \pi^+\pi^-\pi^0$ events. Lines are the fit results.

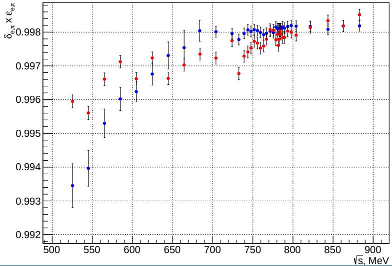

Corrected ID efficiencies for the $e^+e^- \to e^+e^-$ and $e^+e^- \to \pi^+\pi^-$ events

Contribution to the cross section uncertainty

Error	δ_e, %	δ_π at $\sqrt{s} > 0.65$ GeV, %	δ_π at $\sqrt{s} < 0.65$ GeV, %
σ_{stat}	0.01	0.02	0.02 – 0.06
σ_{ID}	0.02	0.01	0.02
σ_{bkg}	0.02	0.02	–
σ_{tot}	0.03	0.03	0.03 – 0.06

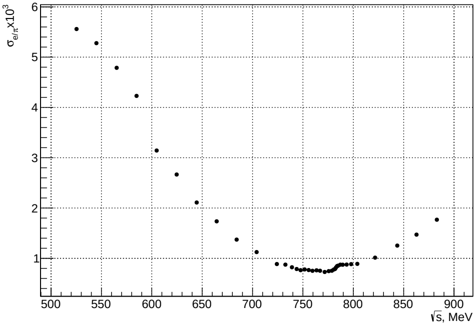

Contribution of the ID efficiencies to the relative error of $e^+e^- \to \pi^+\pi^-$ cross section is **less than 0.2%** for the most energy points

The pseudo–$\pi\pi$ events are used to check the validity of efficiency for the $E_{1,2} > 40$ MeV cut, derived from the simulation

Obtained average correction is equal to **0.992**. The maximum difference between corrections derived from the different types of pseudo-events is **0.5%**

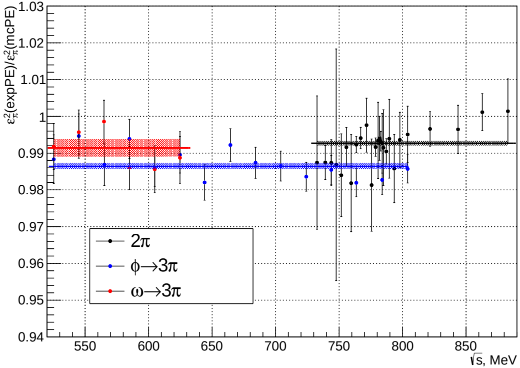

In order to study the differences between simulation and experimental data at each energy point, an efficiency correction is introduced:

$$R_i(x) = \frac{\epsilon_i^{exp}(x)}{\epsilon_i^{mc}(x)} \quad \epsilon_i^{exp} = \frac{N_i(x \in [A_x; B_x])}{N_i(x \in [C_x; D_x])} \quad \epsilon_i^{mc} = \frac{M_i(x \in [A_x; B_x])}{M_i(x \in [C_x; D_x])}$$

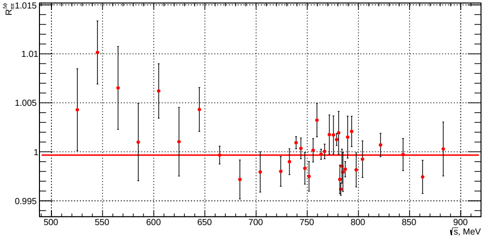

$e^+e^- \to \pi^+\pi^-$

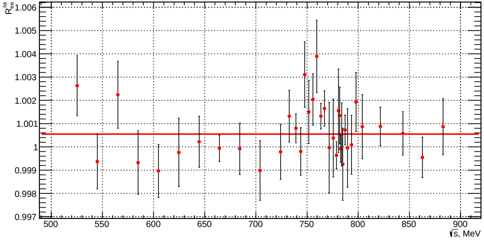

$e^+e^- \to e^+e^-$

Efficiency of the $|\Delta\phi| < 4^\circ$ and $|\Delta\theta| < 12^\circ$ cuts

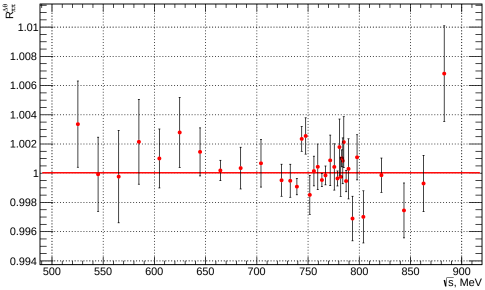

$e^+e^- \to \pi^+\pi^-$

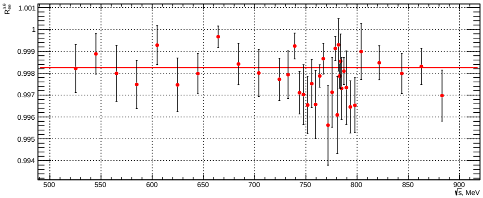

$e^+e^- \to e^+e^-$

The average values of $\delta_{\Delta\phi} = R_{\pi\pi}(\Delta\phi)/R_{ee}(\Delta\phi)$ and $\delta_{\Delta\theta} = R_{\pi\pi}(\Delta\theta)/R_{ee}(\Delta\theta)$ differ from 1 by 0.1 % and 0.2 %, respectively

The overall contribution to the systematic uncertainty from the conditions on the $\Delta\phi$ and $\Delta\theta$ is equal to $0.001 \oplus 0.002 = 0.002$

Efficiency of the $50^\circ < \theta_0 < 130^\circ$ cut

$$R_i(z) = \frac{\varepsilon_i^{exp}(z)}{\varepsilon_i^{mc}(z)} \quad \varepsilon_i^{exp}(z) = \frac{N_i(\theta_0 \in [x; 180^\circ - z])}{N_i(\theta_0 \in [50^\circ; 130^\circ])} \quad \varepsilon_i^{mc}(z) = \frac{M_i(\theta_0 \in [x; 180^\circ - z])}{M_i(\theta_0 \in [50^\circ; 130^\circ])}$$

The statistically significant deviation of $\delta_{\theta_0} = R_{\pi\pi}/R_{ee}$ from unity does not exceed 0.5 %

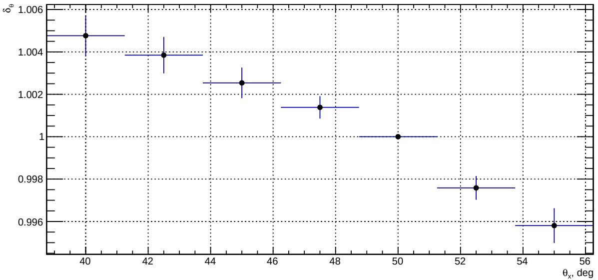

Probability of the π (e) track loss due reconstruction inefficiency is estimated from the $R_{\pi\pi}$ (R_{ee}):

the ratio of the number of events with one track, but the total number of particles > 1 and loosen $\Delta\phi$ and $\Delta\theta$ cuts, to the number of events with two or more tracks

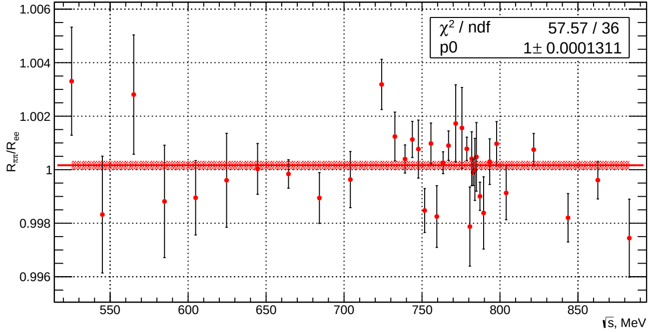

The ratio of $R_{\pi\pi}$ to R_{ee} is taken as a correction to the measured cross section

It does not show a significant deviation from unity

Muon system veto efficiency

$$\delta_{veto} = \frac{\sigma_{\pi\pi}((\phi_1 + \phi_2 - 180^\circ)/2 > 166^\circ or < 14^\circ; veto \geq 0)}{\sigma_{\pi\pi}((\phi_1 + \phi_2 - 180^\circ)/2 > 166^\circ or < 14^\circ; veto = 0)}$$

In case of the *veto* ≥ 0 selection the certain number of the **residual cosmic background** events, derived from the fit of the $(z0_1 + z0_2)/2$ with a sum of uniform and normal distributions, is **subtracted** from the total number of the $e^+e^- \to \pi^+\pi^-$ events

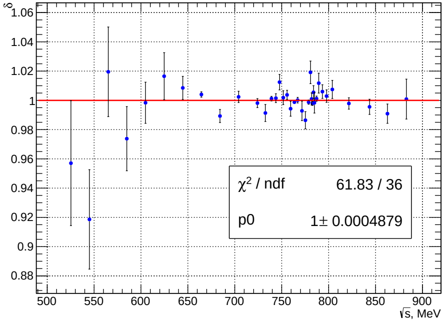

δ_{veto} shows no significant energy dependence

Averaged value is applied and it is consistent with 1

Systematics

The main sources of systematic uncertainty

- $\Delta\theta$, $\Delta\phi$, θ_0 cuts: $0.001 \oplus 0.002 \oplus 0.005 = 0.55\%$
- $E_{1,2} > 40$ MeV condition: 0.5 %
- e/π–separation for the $\sqrt{s} \leq 600$ MeV: 0.3 – 0.5%
- muon subtraction for the $\sqrt{s} \leq 600$ MeV: 0.3 – 0.7%

Additional sources of systematic uncertainty

- 0.2 % is taken as a systematic error from modeling of the pion loss due to nuclear interaction
- Contributions from the $N_{cha} \geq 2$ and $veto = 0$ cuts are considered to be negligible
- Calculation of the radiative correction gives 0.2 % (checked by comparing MCGPJ with BABAYAGA-NLO)

Systematics

Source	$\sqrt{s} > 600$ MeV	$\sqrt{s} \leq 600$ MeV
ID e/π	0.1-0.2	0.3-0.5
μ	0.0-0.2	0.3-0.7
$\Delta\theta$	0.1	
$\Delta\phi$	0.2	
θ_0	0.5	
$E_{1,2}$	0.5	
rad	0.2	
trig	0.1	
nucl	0.2	
total	0.8	0.9-1.2

Calculating $e^+e^- \to \pi^+\pi^-$ cross section

$$N_a = L(\sigma_{\pi\pi}\varepsilon^a_{\pi\pi} + \sigma_{\mu\mu}\varepsilon^a_{\mu\mu} + \sigma_{ee}\varepsilon^a_{ee}) + N^a_{nc}$$

a $=$ 1,2 correspond to the $R_{e/\pi} \in$ [0,1] and $R_{e/\pi} \in$ [- 1,0] respectively; σ_{jj} and ε^a_{jj}, with jj $=$ $\pi^+\pi^-, \mu^+\mu^-, e^+e^-$ in the final state; N^a_{nc} is the number of non-collinear and cosmic background events; L is the IL collected at s_i.

From these equations $e^+e^- \to \pi^+\pi^-$ cross section and L can be deduced:

$$L(s_i) = \frac{(N_2 - N^2_{nc})\varepsilon^1_{\pi\pi} - (N_1 - N^1_{nc})\varepsilon^2_{\pi\pi}}{\sigma_{ee}(\varepsilon^2_{ee}\varepsilon^1_{\pi\pi} - \varepsilon^1_{ee}\varepsilon^2_{\pi\pi}) + \sigma_{\mu\mu}(\varepsilon^2_{\mu\mu}\varepsilon^1_{\pi\pi} - \varepsilon^1_{\mu\mu}\varepsilon^2_{\pi\pi})}$$

$$\sigma_{\pi\pi}(s_i) = \frac{N_1 - N^1_{nc} - L(s_i)\sigma_{\mu\mu}\varepsilon^1_{\mu\mu}(s_i) - L(s_i)\sigma_{ee}\varepsilon^1_{ee}}{L(s_i)\varepsilon^1_{\pi\pi}}$$

Born cross section

$$\sigma^0_{\pi\pi}(s_i) = \frac{\sigma_{\pi\pi}(s_i)}{1+\delta_{rad}(s_i)}$$

$1+\delta_{rad}(s_i)$ is a **radiative correction**, that accounts for radiation from the initial and final states, calculated using the **MCGPJ** code.

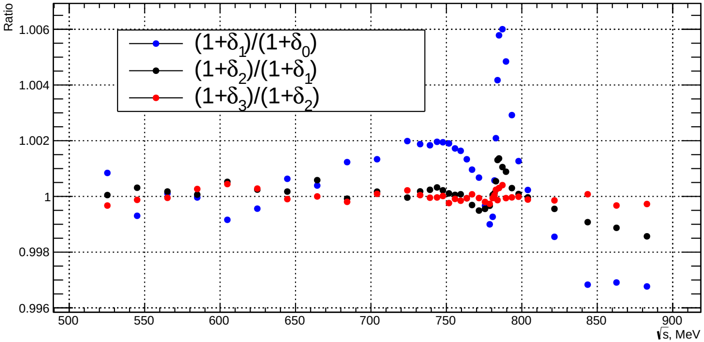

$\delta_{rad}(s_i)$ has to be calculated **iteratively**, by fitting measured cross sections with a model from the MCGPJ

Fit model

$$\sigma_{\pi\pi}(s) = \frac{2}{3}\frac{\alpha^2}{s^{5/2}}P_{\pi\pi}(s)|A_{\pi\pi}(s)|^2$$

$$P_{\pi\pi}(s) = q_\pi^3(s), \qquad q_\pi(s) = \frac{1}{2}\sqrt{s - 4m_\pi^2}$$

$$|A_{\pi\pi}(s)|^2 = \left|\sqrt{\frac{3}{2}\frac{1}{\alpha}}\sum_{V=\rho,\omega,\rho'}\frac{\Gamma_V m_V^3\sqrt{m_V\sigma(V\to\pi^+\pi^-)}}{D_V(s)}\frac{e^{i\phi_{\rho V}}}{\sqrt{q_\pi^3(m_V)}}\right|^2$$

$$D_V(s) = m_V^2 - s - i\sqrt{s}\Gamma_V(s), \quad \Gamma_V(s) = \sum_f \Gamma(V\to f, s)$$

$$\Gamma_\omega(s) = \frac{m_\omega^2}{s}\frac{q_\pi^3(s)}{q_\pi^3(m_\omega)}\Gamma_\omega B_{\omega\to\pi^+\pi^-} + \frac{q_{\pi\gamma}^3(s)}{q_{\pi\gamma}^3(m_\omega)}\Gamma_\omega B_{\omega\to\pi^0\gamma} + \frac{W_{\rho\pi}(s)}{W_{\rho\pi}(m_\omega)}\Gamma_\omega B_{\omega\to3\pi}$$

$$\Gamma_V(s) = \frac{m_V^2}{s}\frac{q_\pi^3(s)}{q_\pi^3(m_V)}\Gamma_V \quad (V=\rho,\rho')$$

Fit results

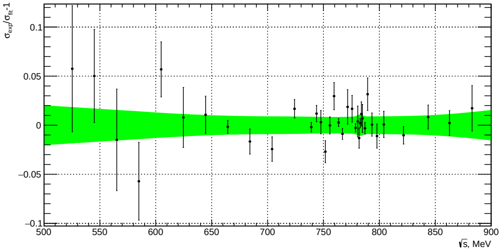

The **relative difference** between the $e^+e^- \to \pi^+\pi^-$ cross section, measured by SND and fit of the SND experimental data. The **green bar** depicts **systematic** and **statistical** errors of the SND fit, folded quadratically.

Cross section values in the $\sqrt{s}$ =751.7, 759.5 and 778.7 MeV energy points shows **non-statistical** deviation from the fit

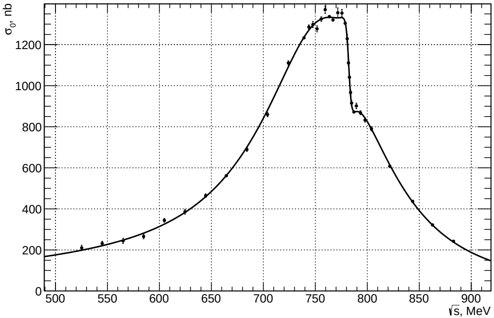

Fit results

Parameter	This work	SND VEPP-2M
m_ρ, MeV	$775.3 \pm 0.5 \pm 0.6$	$774.6 \pm 0.4 \pm 0.5$
Γ_ρ, MeV	$145.6 \pm 0.6 \pm 0.8$	$146.1 \pm 0.8 \pm 1.5$
$\sigma(\rho \to \pi^+\pi^-)$, nb	$1189.7 \pm 4.5 \pm 9.5$	$1193 \pm 7 \pm 16$
$\sigma(\omega \to \pi^+\pi^-)$, nb	$31.5 \pm 1.2 \pm 0.6$	$29.3 \pm 1.4 \pm 1.0$
$\phi_{\rho\omega}$, deg.	$110.7 \pm 1.1 \pm 1.0$	$113.7 \pm 1.3 \pm 2.0$
$\sigma(\rho' \to \pi^+\pi^-)$, nb	2.4 ± 0.6	1.8 ± 0.2
χ^2/ndf	$47/30$	–
$B_{\rho\to e^+e^-} \times B_{\rho\to\pi^+\pi^-}$	$(4.889 \pm 0.015 \pm 0.039) \times 10^{-5}$	$(4.876 \pm 0.023 \pm 0.064) \times 10^{-5}$
$B_{\omega\to e^+e^-} \times B_{\omega\to\pi^+\pi^-}$	$(1.318 \pm 0.051 \pm 0.021) \times 10^{-6}$	$(1.225 \pm 0.058 \pm 0.041) \times 10^{-6}$

Fit results

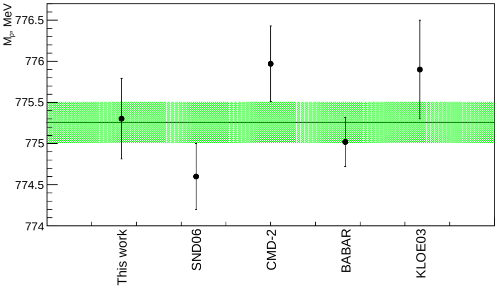

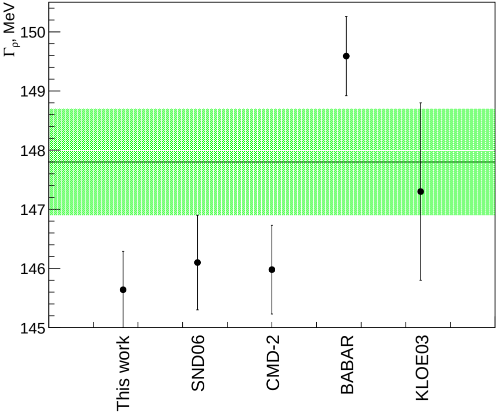

We performed BABAR cross section fit in the energy region 0.525-0.883 GeV using our model. The obtained ρ meson width is **147.38 MeV** $\pm$ **0.47 MeV**.

$$\sigma^{\text{bare}}_{\pi\pi}(s) = \sigma^{0}_{\pi\pi}(s) \times |1 - \Pi(s)|^2 \times \left(1 + \frac{\alpha}{\pi} a(s)\right)$$

$$a(s) = \frac{1+\beta^2}{\beta}\left[4 Li_2\left(\frac{1-\beta}{1+\beta}\right) + 2 Li_2\left(-\frac{1-\beta}{1+\beta}\right) - 3\ln\frac{2}{1+\beta}\ln\frac{1+\beta}{1-\beta} - 2\ln\beta\ln\frac{1+\beta}{1-\beta}\right] - 3\ln\frac{4}{1-\beta^2} - 4\ln\beta + \frac{1}{\beta^3}\left[\frac{5}{4}(1+\beta^2)^2 - 2\right] \times \ln\frac{1+\beta}{1-\beta} + \frac{3}{2}\frac{1+\beta^2}{\beta^2}.$$

$$\mathbf{Li_2(x)} = -\int_0^x dt\,\ln(1-t)/t, \quad \boldsymbol{\beta} = \sqrt{1 - \frac{4m_\pi^2}{s}}$$

LO contribution to a_μ

$$\mathbf{a}_\mu(\pi\pi, s_{min} \leq \sqrt{s} \leq s_{max}) = \left(\frac{\alpha m_\mu}{3\pi}\right)^2 \int_{s_{min}}^{s_{max}} \frac{R(s)K(s)}{s^2} ds$$

$K(s)$ is a known kernel (J. Phys. G **38**, 085003 2011) and

$$R(s) = \frac{\sigma_{\pi\pi}^{bare}}{\sigma(e^+e^- \to \mu^+\mu^-)}, \quad \sigma(e^+e^- \to \mu^+\mu^-) = \frac{4\pi\alpha^2}{3s}$$

Trapezoid integration allows to compute $\mathbf{a}_\mu$ using measured cross sections

Measurement	$a_\mu(\pi\pi) \times 10^{10}$
This work	**409.79 ± 1.44 ± 3.87**
SND VEPP-2M	406.47 ± 1.74 ± 5.28
BaBar	413.58 ± 2.04 ± 2.29
KLOE (combined)	403.39 ± 0.72 ± 2.50

J. High Energ. Phys. 2021, 113 (2021)

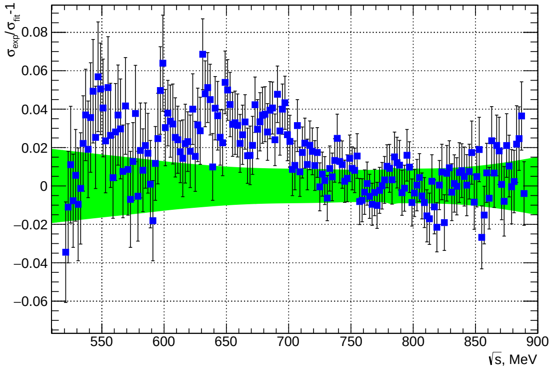

Phys. Rev. 2012.Vol. 86D. 3,032013

The relative difference between the $e^+e^- \to \pi^+\pi^-$ cross section, measured by BABAR and fit of the SND experimental data

- $\sigma_{sys} \oplus \sigma_{stat}$ errors are shown for the BABAR data
- The green bar depicts systematic and statistical errors of the SND fit, folded quadratically

The relative difference between the $e^+e^- \to \pi^+\pi^-$ cross section, measured by KLOE and fit of the SND experimental data

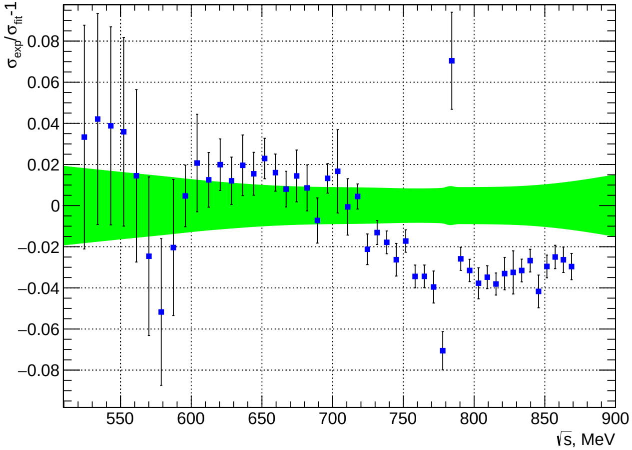

JHEP 1803 (2018) 173

The relative difference between the $e^+e^- \to \pi^+\pi^-$ cross section, measured in experiments at VEPP-2M and fit of the SND experimental data

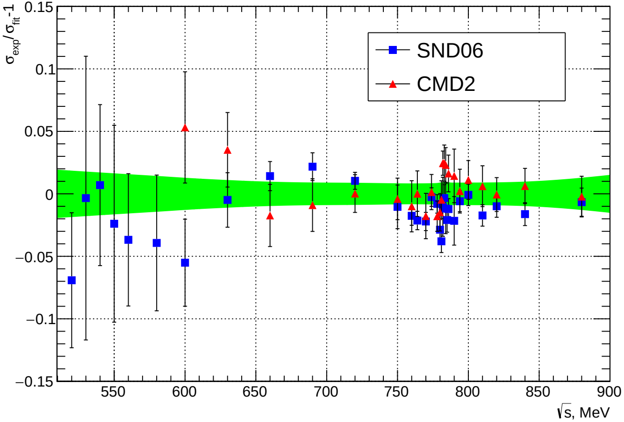

JETP (2006) vol. 103, N3, pp 380-384.

Phys. Lett. 2007 Vol.648B 5. P.28-38

$e^+e^- \to \pi^+\pi^-$ summary

- The difference between the value of $a_\mu(\pi\pi, 525\text{MeV} \leq \sqrt{s} \leq 883\text{MeV})$ obtained from the SND data, and ones derived from the previous measurements $< 1\sigma$
- The parameters of the ρ and ω mesons in this analysis are consistent with ones obtained by SND in experiments at VEPP-2M
- Comparison with VEPP-2M results indicates no significant contradictions in the whole energy spectrum
- In the $0.6 \leq \sqrt{s} \leq 0.7$ GeV energy range there is a 3% discrepancy between the SND and BABAR data, but for the rest of the spectrum SND data is in agreement with the BABAR results
- There is 1–4 % difference between KLOE and SND data for $\sqrt{s} \geq 0.7$ GeV

Conclusion

- The $\mathbf{e^+e^-} \to \pi^+\pi^-$ cross section is measured with systematic uncertainty **better then 1%** using a small fraction of collected data.
- The $\mathbf{e^+e^-} \to \pi^+\pi^-\pi^0$ process is studied at $\sqrt{s} > 1.05$ GeV.
- $\mathbf{e^+e^-} \to \phi\pi^0 \to \mathbf{K^+K^-}\pi^0$ cross section indicates a presence of new resonance with $\mathbf{m = 1585 \pm 15MeV}$ and $\mathbf{\Gamma = 75 \pm 30MeV}$.
- Rare radiative process $\mathbf{e^+e^-} \to \mathbf{a_0(1450)}\gamma$ have been measured for the first time in the $\eta\pi^0\gamma$ channel.
- Search for production of the C-even resonance $f_1(1285)$, in e^+e^- annihilation is performed. The **first indication** of the process $\mathbf{e^+e^-} \to \mathbf{f_1(1285)}$ is obtained.

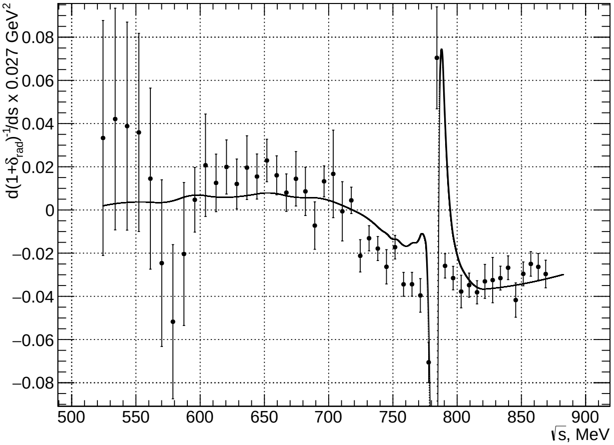

d(1+δ_rad)^-1/ds x 0.027 GeV^2
0.08
0.06
0.04
0.02
0
−0.02
−0.04
−0.06
−0.08
500
550
600
650
700
750
800
850
900
√s, MeV

$\sqrt{s}$, MeV	$\sigma_{\pi\pi}$, nb	$\sigma^0_{\pi\pi}$, nb	$\lvert F(s)\rvert^2$	$1+\delta_{rad}$	σ_{pol}, nb
525.07	203.4±12.3±2.4	210.4±12.7±2.5	4.4±0.3±0.1	0.967	209.7±12.7±2.5
543.99	224.4±10.1±2.5	232.5±10.5±2.6	5±0.2±0.1	0.965	231.9±10.4±2.6
565.2	235±12.3±2.4	244.3±12.8±2.5	5.5±0.3±0.1	0.962	243.8±12.8±2.5
585.04	254.2±10.7±2.5	265±11.1±2.6	6.2±0.3±0.1	0.959	264.8±11.1±2.6
604.85	328.8±8.7±3	344.7±9.2±3.1	8.3±0.2±0.1	0.954	344.8±9.2±3.1
624.78	366.4±11.1±3.2	386.1±11.7±3.4	9.7±0.3±0.1	0.949	386.7±11.7±3.4
644.63	438±8.2±3.7	464.2±8.7±3.9	12.1±0.2±0.1	0.944	465.6±8.7±3.9
664.53	525.9±3.5±4.4	561.3±3.7±4.7	15.3±0.1±0.1	0.937	563.7±3.7±4.7
684.42	642.1±8.4±5.3	689.1±9±5.6	19.5±0.3±0.2	0.932	692.9±9.1±5.7
704.21	798.1±10.3±6.5	860.7±11.1±7	25.4±0.3±0.2	0.927	865.5±11.1±7
724.12	1030.4±9.5±8.3	1112.6±10.3±9	34.2±0.3±0.3	0.926	1116.6±10.3±9
739.13	1146.5±5.6±9.2	1233.7±6±9.9	39.1±0.2±0.3	0.929	1234±6±9.9
743.8	1200.9±9.8±9.7	1289.4±10.6±10.4	41.3±0.3±0.3	0.931	1288.1±10.6±10.4
747.74	1215±14.4±9.8	1301.6±15.4±10.5	42±0.5±0.3	0.933	1298.7±15.4±10.5
751.71	1199.4±13.7±9.7	1281.4±14.7±10.3	41.7±0.5±0.3	0.936	1276.6±14.6±10.3
755.7	1246.5±10.8±10	1327.9±11.5±10.7	43.5±0.4±0.4	0.939	1321.3±11.4±10.6
759.58	1288.3±17.3±10.4	1368±18.3±11	45.2±0.6±0.4	0.942	1360.3±18.2±10.9
763.63	1263.4±5±10.2	1336.8±5.2±10.8	44.5±0.2±0.4	0.945	1328.9±5.2±10.7
767.83	1249.1±6.9±10.1	1317±7.2±10.6	44.2±0.2±0.4	0.948	1310±7.2±10.5
771.57	1290.3±22.2±10.4	1356.5±23.3±10.9	45.9±0.8±0.4	0.951	1351.7±23.2±10.9
775.73	1290.9±17.2±10.4	1353.6±18±10.9	46.2±0.6±0.4	0.954	1353.2±18±10.9
778.55	1257±5.3±10.1	1311.1±5.5±10.5	45±0.2±0.4	0.959	1307.4±5.5±10.5
780.74	1199±18.4±9.7	1229.2±18.9±9.9	42.3±0.7±0.3	0.976	1211.4±18.6±9.8

782.03	1104.8±11.2±8.9	1106.9±11.2±8.9	38.2±0.4±0.3	0.998	1074.7±10.9±8.7
782.9	1058.1±4.8±8.5	1039.8±4.7±8.4	36±0.2±0.3	1.017	999±4.5±8
783.72	1004.9±11.6±8.1	971.9±11.3±7.8	33.7±0.4±0.3	1.033	925.2±10.7±7.5
784.7	959.2±12.8±7.7	916.8±12.2±7.4	31.9±0.4±0.3	1.046	865.8±11.6±7
786.7	913.5±5.1±7.4	872.3±4.8±7	30.4±0.2±0.2	1.047	819.1±4.5±6.6
789.45	934.6±14.1±7.5	903.1±13.7±7.3	31.7±0.5±0.3	1.035	850.9±12.9±6.9
793.91	890.4±10±7.2	867.8±9.7±7	30.7±0.3±0.2	1.026	823.1±9.2±6.6
797.66	858.9±10.1±6.9	836.3±9.9±6.7	29.8±0.4±0.2	1.027	795.8±9.4±6.4
803.98	819.5±10.5±6.6	791.4±10.1±6.4	28.6±0.4±0.2	1.036	755.4±9.6±6.1
821.79	654.8±5.6±5.3	608.7±5.2±4.9	22.8±0.2±0.2	1.076	583±5±4.7
843.36	496.6±5.8±4	438±5.1±3.6	17.1±0.2±0.1	1.134	420.4±4.9±3.4
862.68	382.2±4.6±3.1	321.2±3.9±2.6	13±0.2±0.1	1.19	309±3.7±2.5
883.19	303.2±6.7±2.5	242.1±5.3±2	10.2±0.2±0.1	1.252	233.5±5.1±1.9